

Compressive behaviour of high strength steel cross-sections

Gkantou, Michaela; Theofanous, Marios; Antoniou, Nikolaos; Baniotopoulos, Charalampos

DOI:

[10.1680/jstbu.16.00101](https://doi.org/10.1680/jstbu.16.00101)

License:

Other (please specify with Rights Statement)

Document Version

Publisher's PDF, also known as Version of record

Citation for published version (Harvard):

Gkantou, M, Theofanous, M, Antoniou, N & Baniotopoulos, C 2017, 'Compressive behaviour of high strength steel cross-sections', *Institution of Civil Engineers. Proceedings. Structures and Buildings*.
<https://doi.org/10.1680/jstbu.16.00101>

[Link to publication on Research at Birmingham portal](#)

Publisher Rights Statement:

Version of record is published in Proceedings of the ICE - Structures and Buildings

<http://www.icevirtuallibrary.com/doi/10.1680/jstbu.16.00101>

General rights

Unless a licence is specified above, all rights (including copyright and moral rights) in this document are retained by the authors and/or the copyright holders. The express permission of the copyright holder must be obtained for any use of this material other than for purposes permitted by law.

- Users may freely distribute the URL that is used to identify this publication.
- Users may download and/or print one copy of the publication from the University of Birmingham research portal for the purpose of private study or non-commercial research.
- User may use extracts from the document in line with the concept of 'fair dealing' under the Copyright, Designs and Patents Act 1988 (?)
- Users may not further distribute the material nor use it for the purposes of commercial gain.

Where a licence is displayed above, please note the terms and conditions of the licence govern your use of this document.

When citing, please reference the published version.

Take down policy

While the University of Birmingham exercises care and attention in making items available there are rare occasions when an item has been uploaded in error or has been deemed to be commercially or otherwise sensitive.

If you believe that this is the case for this document, please contact UBIRA@lists.bham.ac.uk providing details and we will remove access to the work immediately and investigate.

Compressive behaviour of high-strength steel cross-sections

Gkantou, Theofanous, Antoniou and Baniotopoulos

ice | proceedings

http://dx.doi.org/10.1680/jstbu.16.00101

Paper 1600101

Received 06/05/2016

Accepted 08/05/2017

Keywords: codes of practice & standards/design methods & aids/ steel structures

ICE Publishing: All rights reserved

Compressive behaviour of high-strength steel cross-sections

Michaela Gkantou MSc, PhD

Research Fellow, School of Engineering, Department of Civil Engineering, University of Birmingham, Birmingham, UK (corresponding author: m.gkantou@bham.ac.uk)

Marios Theofanous MSc, DIC, PhD

Lecturer, School of Engineering, Department of Civil Engineering, University of Birmingham, Birmingham, UK

Nikolaos Antoniou MSc

Structural Engineer, Basler & Hofmann, Switzerland; formerly Research Fellow, School of Engineering, Department of Civil Engineering, University of Birmingham, UK

Charalampos Baniotopoulos MSc, PhD

Professor HC, School of Engineering, Department of Civil Engineering, University of Birmingham, Birmingham, UK

The recent increase in the use of high-strength steels (HSSs) in modern engineering practice necessitates a deeper understanding of their structural response. Given that HSS design specifications are largely based on a limited number of test data and assumed analogies with mild steel, their applicability to HSS sections needs to be assessed. In the work reported in this paper, finite-element models were developed and validated against experimental data of hot-finished S460 and S690 grade steel stub columns. Parametric studies were conducted to generate a large volume of structural performance data over a wide range of cross-section slenderness values and aspect ratios. On the basis of the results, the suitability of the Eurocode 3 (EC3) class 3 slenderness limit and the effective width equations for HSS sections were assessed. Aiming to account for element interaction effects, which are not considered in EC3, an effective cross-section method applicable to HSS slender sections was developed. Finally, the continuous-strength method was extended to stocky S460 sections, for which overly conservative strength predictions were observed. The reliability of the proposed design methods was verified according to annex D of the Eurocode structural design basis (EN 1990).

Notation

A	cross-sectional area
A_c	cross-sectional area of corners
A_{eff}	effective cross-sectional area
B	width
b	width of internal element
b_c	centreline width
b_{eff}	effective width
b_f	width of flange
b_w	width of web
\bar{b}	average ratio of test (or finite element (FE)) to model resistance
C, D	coefficients in the proposed effective cross-section method
clt_e	slenderness of the most slender constituent plate element
E	Young's modulus
E_{sh}	Young's modulus of the strain-hardening region
f_{cr}	elastic critical buckling stress
f_{CSM}	continuous strength method (CSM) ultimate stress
f_u	ultimate stress
f_y	yield stress
H	depth
H/B	cross-section aspect ratio
h_c	centreline depth
k_b	buckling coefficient in Seif and Schafer (2010)
k_c	buckling coefficient in Eurocode 3
$k_{d,n}$	design (ultimate limit state) fractile factor
M_u	ultimate (failure) moment
N_u	ultimate (failure) load

n	number of tests and FE simulations
t	plate thickness
V_r	combined coefficient of variation (CoV) incorporating both model and basic variable uncertainties
V_δ	CoV of the tests and FE simulations relative to the resistance model
β	coefficient determined by Gardner <i>et al.</i> (2010)
γ_{M0}	partial safety factor for cross-section resistance
ϵ_{CSM}	strain at ultimate load according to CSM
ϵ_{eng}	engineering strain
$\epsilon_{\text{ln}}^{\text{pl}}$	logarithmic plastic strain
ϵ_u	strain at ultimate load
ϵ_y	strain at yield load
$\bar{\lambda}_{\text{CS}}$	cross-section slenderness
$\bar{\lambda}_p$	plate slenderness
$\bar{\lambda}_w$	web slenderness
ν	Poisson's ratio
ρ	reduction factor for the plate element
ρ_{CS}	reduction factor for the cross-section
ρ_f	reduction factor for the flange
ρ_w	reduction factor for the web
σ_{eng}	engineering stress
σ_{true}	true stress
ω_{DW}	initial geometric imperfection according to Dawson and Walker (1972)
ω_0	largest measured initial geometric imperfection

1. Introduction

Advances in production technology of high-strength steel (HSSs) have allowed HSSs with improved ductility and

weldability to be produced at a lower cost, thereby rendering HSS an attractive material for structural applications. The enhanced material strength generally leads to smaller section sizes, thus resulting in lighter, more elegant structures, reduced transportation and erection costs and reduced carbon dioxide footprint, with profound sustainability benefits. In order to maximise the potential benefits of HSSs and increase their usage in the construction industry, appropriate design guidance in line with observed structural responses needs to be available. In Europe, the design of HSS (i.e. steels with a yield strength higher than 460 N/mm² and up to 700 N/mm²) structures is covered by EN 1993-1-12 (CEN, 2007), which refers back to 1993-1-1 (CEN, 2005) for most design checks, but also specifies additional design rules to account for the reduced ductility and strain-hardening characteristics of such steels. Similarly, other structural steel codes (ANSI/AISC 360-10 (AISC, 2010), AISI S100-12 (AISI, 2012) and AS 4100-A1 (Standards Australia, 2012)) have incorporated the use of HSS within their guidance. Given that HSS design provisions are largely based on test data for mild steel and the recommended rules and methods for HSS are identical to those for normal-strength steel, further investigation on the applicability of such design specifications to HSS is required.

Numerous experimental and numerical programmes have been conducted in attempts to evaluate the structural response of HSS at cross-sectional and member level. Investigations into the cross-sectional response through the execution of stub column tests, which is the focus of the current study, date back to 1966 when Nishino *et al.* (1966) tested stub columns built-up from welded A514 plates ($f_y \approx 690$ N/mm²) and compared their response to that of normal-strength steel counterparts. Two decades later, the local buckling of sections comprising HSS plates was studied by Usami and Fukumoto (1984). The applicability of the Australian yield slenderness limit (i.e. transition limit from fully effective sections to sections with reduced effectiveness) to HSS sections was studied by Rasmussen and Hancock (1992), who investigated the response of Bisalloy 80 ($f_y = 690$ N/mm²) stub columns. Yuan (1997) tested HSS wide-flange beam sections to assess the applicability of slenderness limits to HSS. Yang and Hancock (2004) performed a series of compression tests on cold-formed G550 ($f_y = 550$ N/mm²) stub columns in order to evaluate the influence of the decreased strain-hardening material characteristics on the compression capacity, whereas Gao *et al.* (2009) studied the influence of the width-to-thickness ratio and the cross-section aspect ratio on the ultimate load-carrying capacity of thin-walled box columns with $f_y \approx 745$ –800 N/mm². The local buckling response of HSA 800 ($f_u = 800$ N/mm²) box and I-sections was investigated by Yoo *et al.* (2013), and the results of concentric stub column tests on sections of the same material were utilised to assess Korean stability criteria (Kim *et al.*, 2014). Two more series of experimental investigations on stub columns with a nominal yield strength of 460 N/mm² were executed in order to evaluate the applicability of various

international design codes to HSS (Shi *et al.*, 2014; Zhou *et al.*, 2013a), while Shi *et al.* (2016) recently numerically studied the ultimate behaviour of normal-strength and HSS welded sections.

Complementing the published studies on the applicability of current design provisions to HSS sections, this paper describes an investigation into the structural behaviour of S460 and S690 hot-finished square hollow sections (SHSs) and rectangular hollow sections (RHSs) and provides relevant design recommendations.

2. Numerical modelling

The general-purpose finite-element (FE) software Abaqus (Hibbit, Karlsson & Sorensen Inc., 2010) was used to execute the numerical modelling described in this section. The developed FE models were validated against the experimental results of S460 and S690 concentrically loaded stub columns reported by Wang *et al.* (2017). The validated numerical models were subsequently used for the execution of extensive parametric studies, which enabled the investigation of the structural response of HSS RHSs with varying cross-section slenderness values and aspect ratios.

2.1 Brief description of the experimental programme

In order to study the structural response of hot-finished HSS sections in compression, a comprehensive experimental programme comprising 11 concentric stub columns was performed (Wang *et al.*, 2017). The tested sections were hot-rolled seamlessly from continuously cast round ingots and hollowed out in a piercing mill to their final section shape. High strength in the S460 sections was achieved by means of the normalising process, while a quenching and tempering process was used for S690. An initial series of coupon tests provided the material stress–strain response, which exhibited a distinct yield plateau followed by a strain-hardening range, more pronounced in S460 than S690. Typical stress–strain curves obtained from the tensile coupon tests are depicted in Figure 1. For grade S460,

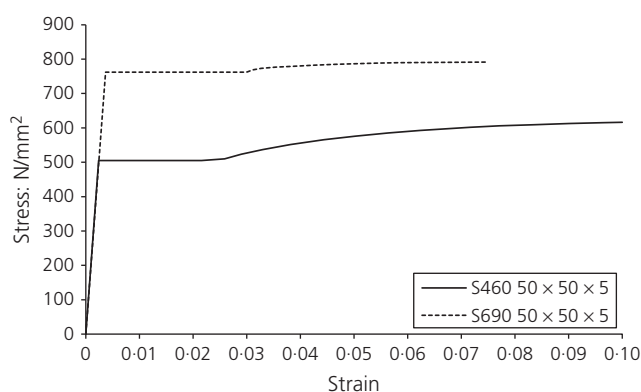


Figure 1. Typical stress–strain curves from tensile flat coupon tests (Wang *et al.*, 2016)

Table 1. Summary of the concentric stub column tests (Wang *et al.*, 2017)

Cross-section	$N_{u,Exp}$: kN	ω_0 : mm	$\frac{N_{u,Exp}}{Af_y}$
S460 50 × 50 × 5	645.16	0.054	1.59
S460 50 × 50 × 4	477.63	0.043	1.45
S460 100 × 100 × 5	1042.29	0.077	1.14
S460 90 × 90 × 3.6	628.34	0.083	1.05
S460 100 × 50 × 6.3	1188.45	0.049	1.47
S460 100 × 50 × 4.5	713.26	0.070	1.20
S690 50 × 50 × 5	804.04	0.076	1.27
S690 100 × 100 × 5.6	1673.94	0.081	1.05
S690 90 × 90 × 5.6	1511.56	0.089	1.07
S690 100 × 50 × 6.3	1409.59	0.106	1.08
S690 100 × 50 × 5.6	1212.21	0.156	1.05

the average obtained values for the yield strength (f_y) and ultimate tensile stress (f_u) were 484 N/mm² and 643 N/mm², respectively, while the respective average values for S690 were 764 N/mm² and 802 N/mm². Having established the material behaviour, six S460 and five S690 stub columns were concentrically loaded to failure. Table 1 gives the nominal dimensions of the tested specimens and a summary of the test results. Further details on the measured dimensions and the fabrication process of the specimens and the experimental procedure are provided in Wang *et al.* (2017). As anticipated, the most dominant failure type was local buckling. The elephant-foot failure mode, owing to the friction between the ends of the specimen and loading plates, was noticed in some stocky sections with very low imperfection magnitudes. It should be noted that all the specimens failed at loads beyond their squash load.

2.2 Modelling assumptions

In line with past studies (Wang *et al.*, 2016; Zhou *et al.*, 2013a) that employed the four-noded doubly curved shell element S4R with reduced integration and finite membrane strains for the development of FE models capable of efficiently capturing cross-sectional performance, this element type was used for the development of the FE models described in this paper. An initial mesh convergence study revealed that an average element size equal to the thickness of the modelled component was sufficient to accurately replicate the experimentally observed structural behaviour within a reasonable computational time. All degrees of freedom were restrained at both ends of the modelled stub columns except for the axial translation of the loaded end, where an incremental axial displacement was applied.

The material properties employed in the numerical models were based on the stress–strain curves recorded from tensile flat coupon tests. An elastic–plastic model with von Mises yield criterion and isotropic hardening was adopted. Equations 1 and 2 were applied for the conversion of the measured engineering stress–strain curves to true stress–logarithmic plastic

strain curves before their input into the software

$$1. \quad \sigma_{true} = \sigma_{eng}(1 + \varepsilon_{eng})$$

$$2. \quad \varepsilon_{ln}^{pl} = \ln(1 + \varepsilon_{eng}) - \frac{\sigma_{true}}{E}$$

where σ_{eng} and ε_{eng} are the engineering stress and strain respectively, E is the Young's modulus and σ_{true} and ε_{ln}^{pl} are the true stress and logarithmic plastic strain, respectively.

Buckling is triggered in real members by the initial geometric imperfections inherently present. In order to ensure adequate replication of the experimentally observed response, the initial geometric imperfections need to be explicitly incorporated in the numerical models. In accordance with similar studies (Wang *et al.*, 2016; Zhou *et al.*, 2013a), an effective and easy representation of the real geometric imperfection pattern can be obtained through the incorporation of the elastic buckling mode shape corresponding to the lowest elastic critical buckling load. In addition to the shape of the initial geometric imperfections, their magnitude is of significant importance when simulating any type of buckling. In the current study, the following six local imperfection magnitudes were considered: no imperfection, $t/100$, $t/50$, $t/10$, the maximum measured imperfection (ω_0) as reported by Wang *et al.* (2017) and shown in Table 1 and an imperfection amplitude proposed by Dawson and Walker (1972) and modified by Gardner and Nethercot (2004), as defined by

$$3. \quad \omega_{DW} = \beta \sqrt{\frac{f_y}{f_{cr}}} t$$

where f_y is the yield strength of the plate material, f_{cr} is the theoretical local buckling stress of the most slender constituent element of the section, t is the plate thickness and $\beta = 0.028$, as proposed for carbon steel hot-rolled RHSs by Gardner *et al.* (2010).

In addition to the initial geometric imperfections, the residual stresses arising during the forming process may influence the ultimate structural performance of components failing by buckling. Wang *et al.* (2016) measured and reported the residual stress patterns and magnitudes for hot-finished HSS sections. The magnitudes of the recorded residual stresses were found to be 5.5% and 3.1% of the yield strength f_y for the tensile and compressive residual stresses, respectively. Due to their very low magnitudes compared with the material yield strength, it was decided not to explicitly introduce residual stresses in the FE models.

Having developed the numerical models for the concentric stub columns, a non-linear static analysis using the modified Riks procedure and taking due account of material and

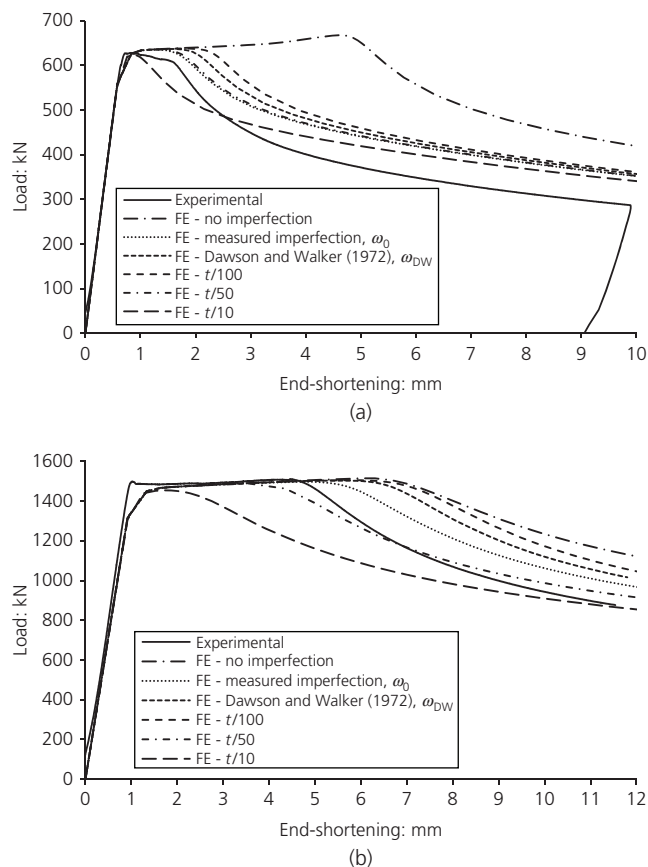


Figure 2. Experimental and numerical load–end-shortening curves for various initial local geometric imperfection amplitudes: (a) S460 90 × 90 × 3.6; (b) S690 90 × 90 × 5.6

geometric non-linearities (Hibbit, Karlsson & Sorensen Inc., 2010) was performed. The full load–displacement path was traced and the ultimate loads together with the corresponding end-shortenings were obtained.

2.3 Validation of the FE models

In order to ensure that the FE models could accurately predict the structural response of HSS stub columns, the experimental stiffness, ultimate load, overall response and failure mode reported by Wang *et al.* (2017) had to be accurately replicated by the FE models. To this end, the numerical load–end-shortening curves were compared with the experimental results (Figure 2) for SHSs 90 × 90 × 3.6 in grade S460 and 90 × 90 × 5.6 in grade S690. The effect of the magnitude of initial geometric imperfections on the ultimate load and the post-ultimate response can be seen in Figure 2. Typical experimental and numerical failure modes classified as local buckling and elephant-foot buckling are shown in Figure 3. The ratios of numerical to experimental ultimate loads ($N_{u,FE}/N_{u,Exp}$) for varying imperfection magnitudes are listed in Table 2, where a fairly accurate numerical prediction of the ultimate load capacity for all of the considered initial geometric imperfection amplitudes can be observed.

It should be noted that the present research work was part of a series of studies investigating the cross-sectional performance of S460 and S690 steel grades. Three series of experimental and numerical studies were performed: three-point and four-point bending tests (Wang *et al.*, 2016), eccentrically loaded stub column tests (Gkantou *et al.*, 2017) and concentric stub column tests. In all cases, the numerically obtained load–deformation response for six different considered imperfection

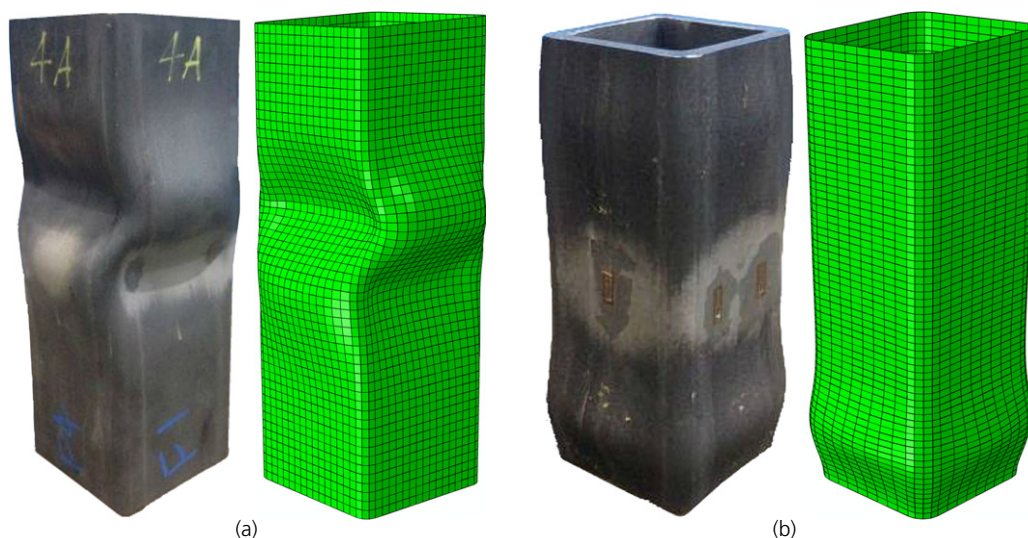


Figure 3. Typical experimental and numerical failure modes: (a) local buckling (S460 90 × 90 × 3.6); (b) elephant-foot buckling (S690 50 × 50 × 5)

Table 2. Comparison of FE and test data for different levels of imperfection

Cross-section	$N_{u,FE}/N_{u,Exp}$					
	No imperfection	Measured imperfection, ω_0	ω_{DW}	$t/100$	$t/50$	$t/10$
S460 50 × 50 × 5	0.95	0.93	0.95	0.95	0.93	0.95
S460 50 × 50 × 4	0.93	0.89	0.91	0.88	0.85	0.75
S460 100 × 100 × 5	1.05	0.96	0.96	0.96	0.96	0.94
S460 90 × 90 × 3.6	1.06	1.01	1.01	1.02	1.01	0.99
S460 100 × 50 × 6.3	0.99	1.02	1.01	1.01	0.95	0.86
S460 100 × 50 × 4.5	0.94	0.97	0.97	0.98	0.94	0.88
S690 50 × 50 × 5	0.90	0.90	0.90	0.90	0.90	0.83
S690 100 × 100 × 5.6	1.01	1.00	1.00	1.00	1.00	0.98
S690 90 × 90 × 5.6	1.00	0.99	1.00	1.00	0.99	0.96
S690 100 × 50 × 6.3	1.04	1.01	1.02	1.02	0.99	0.94
S690 100 × 50 × 5.6	1.01	0.99	1.00	1.03	1.00	0.97
Mean	0.99	0.97	0.98	0.98	0.96	0.91
CoV	0.05	0.05	0.04	0.05	0.05	0.08

magnitudes (i.e. no imperfection, ω_0 , ω_{DW} , $t/100$, $t/50$ and $t/10$) was compared with the experimental one. In order to maintain consistency, one imperfection magnitude able to give the best replication in all three studies was selected for execution of the subsequent parametric studies. On the basis of the numerical/experimental ratios of ultimate loads, it was found that the imperfection magnitude able to give overall the best agreement with the experimental results was $t/50$ (i.e. $M_{u,FE}/M_{u,EXP}$ equal to 1.01 and 0.99 in three-point and four-point beams, respectively (Wang *et al.*, 2016) and equal to 0.98 in eccentric stub columns (Gkantou *et al.*, 2017)). As shown in Table 2, the imperfection magnitude of $t/50$ resulted in a mean value of $N_{u,FE}/N_{u,EXP}$ equal to 0.96 with a coefficient of variation (CoV) of 0.05, which was deemed a slightly conservative but sufficiently accurate prediction of the ultimate response of concentric stub columns and could therefore be used for the execution of parametric studies.

2.4 Parametric studies

Having validated the FE models against the test results, thorough parametric studies were conducted to generate additional structural performance data that would allow an in-depth understanding of the cross-sectional response and a meticulous evaluation of relevant design specifications. Six cross-section aspect ratios ($H/B=1.00$, 1.25, 1.50, 2.00, 2.50 and 3.00) were studied in order to investigate the effect of the plate element interaction on the cross-sectional response of HSS sections. Both S460 and S690 steel grades were considered in order to study the effect of the strain-hardening material properties. Maintaining the cross-section outer dimensions and varying the cross-section thickness, cross-sections with a c/t ratio ranging from 10 to 100 were modelled, where c is the compressed flat width, t is the plate thickness and $\varepsilon=(235/f_y)^{1/2}$. In line with past studies (Bock and Real, 2015; Gardner and Nethercot, 2004; Wang *et al.*, 2016), the average

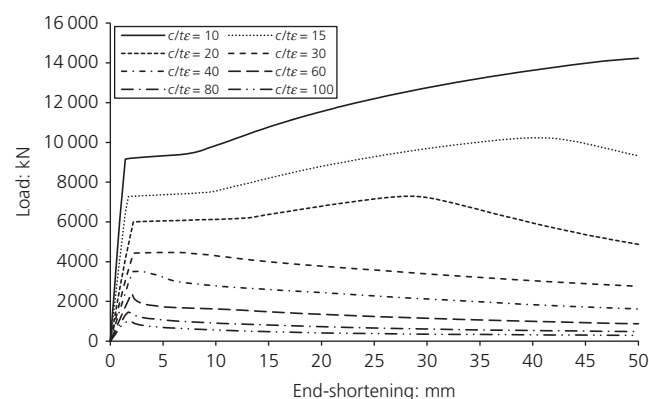


Figure 4. Typical load–end-shortening curves for S460 RHS with an aspect ratio of 3.00 and various values of plate slenderness

material properties obtained for each steel grade from tensile coupon tests (Wang *et al.*, 2016) were incorporated in the FE models. The length of the specimens was set equal to three times the largest cross-section dimension, thus allowing for sufficient representation of the initial local geometric imperfection pattern but excluding global buckling failure mode (Galambos, 1998). An imperfection magnitude of $t/50$ was introduced in the form of the lowest elastic buckling mode shape.

The failure load, the corresponding end-shortening and the full load–displacement path were recorded for each analysis. Typical curves of the load–end-shortening response are given in Figure 4. As anticipated, the stocky sections exhibited significant strain-hardening before reaching their ultimate load, whereas local buckling led to failure at average compressive strains within the elastic range for slender sections. Typical elastic critical buckling mode shapes and failure modes are depicted in Figure 5.

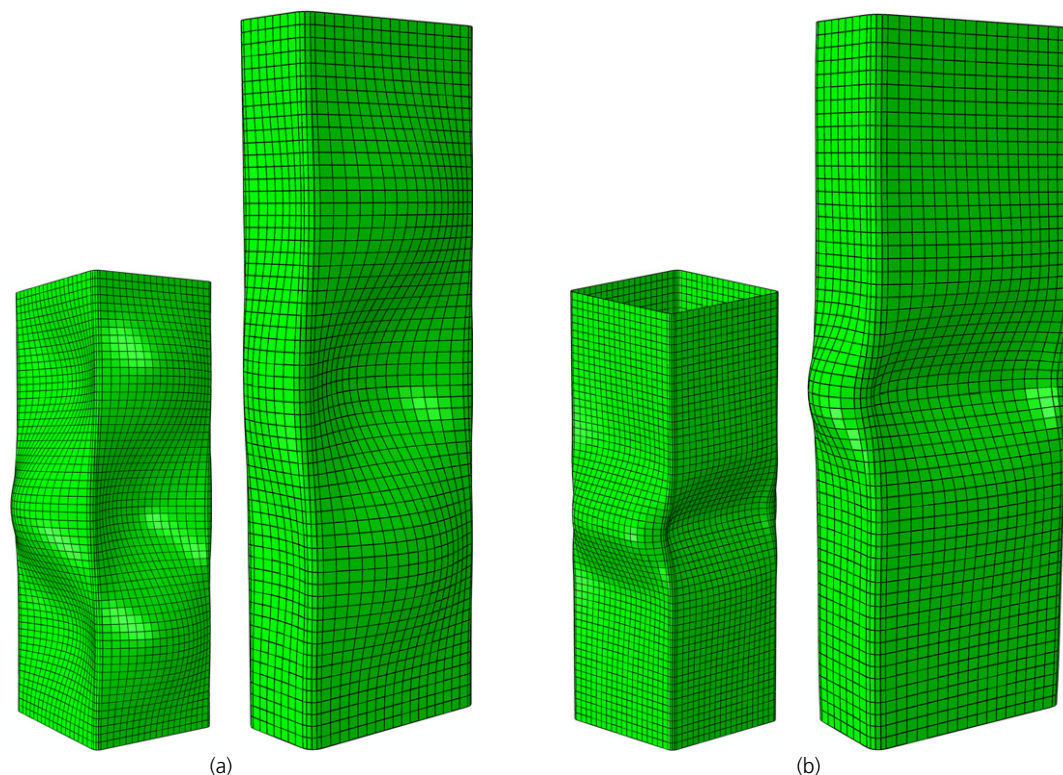


Figure 5. Typical numerical elastic critical buckling mode shapes and failure modes: (a) elastic critical buckling mode shapes (SHS, RHS); (b) failure modes (SHS, RHS)

3. Analysis of the results and design recommendations

In this section, the results of the parametric studies are presented and used to assess various design specifications. The suitability of the Eurocode 3 (EC3) class 3 slenderness limit for internal elements in compression and the effective width equations for HSS sections is initially assessed. Thereafter, the design of slender sections incorporating the effect of element interaction is attempted by proposing an effective cross-section rather than an effective width approach. Finally, the applicability of the continuous strength method (CSM) for the design of stocky cross-sections in grade S460, which exhibit significant strain-hardening, is assessed. Appropriate design recommendations are made and new equations to make the design methods applicable to hot-finished HSS sections are proposed.

3.1 EC3 class 3 limit and effective width equations

Eurocode 3 (EN 1993-1-12 (CEN, 2007) referring to 1993-1-1 (CEN, 2005)) adopts the concept of the cross-section classification in order to treat local buckling. Comparing the width-to-thickness ratio of the constituent plate elements to the codified plate slenderness limits, a structural cross-section can be classified into four classes, with the cross-sectional response

being related to the class of the most slender plate element. The codified plate slenderness limits vary depending on the stress distribution, the material properties and the boundary conditions of the assembly plate elements. Given that the same limits with mild steel have been adopted for HSS, the applicability to HSS needs to be examined.

The EC3 class 3 slenderness limit defines the transition from a fully effective (i.e. class 1–3) to a slender (i.e. class 4) section. Class 1–3 sections can attain their yield load capacity under pure compression, while class 4 sections fail by local buckling before their squash load is reached. In order to assess the codified slenderness limit for internal elements in compression, the ultimate load capacities of the studied concentric stub columns of the two steel grades considered were normalised by the respective squash loads (Af_y) and plotted against the slenderness of the most slender constituent plate element (c/t_e). The results are shown in Figure 6(a), where the current class 3 limit of 42 is also shown. The figure reveals that sections of slenderness less than 42 fail at or beyond their squash load, showing that the codified slenderness limit is applicable to hot-finished S460 and S690 hollow sections. Moreover, for cross-sections of the same aspect ratio, the steel grade has no obvious influence on the normalised performance of slender sections, which fail within the elastic range, while it does affect the response of

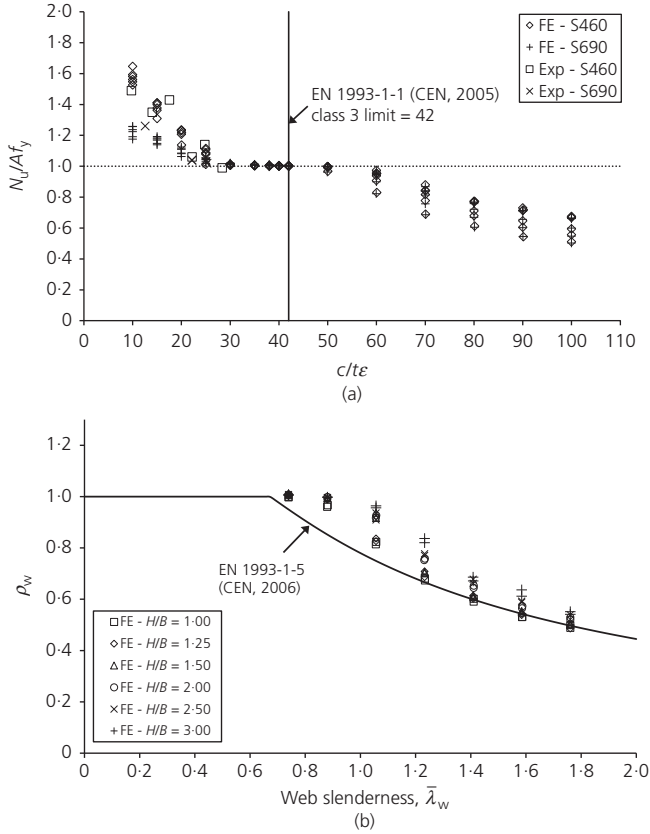


Figure 6. Assessment of the EC3 design provisions: (a) class 3 limit for internal elements in compression; (b) effective width equations

sections in the stocky range. The strength predictions for the stocky sections were conservative; this is more pronounced for the S460 sections than their S690 counterparts and is due to the Eurocode assumption of an elastic-perfectly plastic material response that ignores strain-hardening material properties.

In order to account for the loss of effectiveness due to local buckling occurring in class 4 sections, the traditional effective width method is employed by EN 1993-1-12 (CEN, 2007). For internal elements in compression with $b/t\epsilon > 42$, Equation 4 is used to estimate the effective width (b_{eff}) (EN 1993-1-5 (CEN, 2006)), where ρ is the reduction factor given from Equations 5 and 6, $\bar{\lambda}_p$ is the plate slenderness given by Equation 7 and k_c is the buckling coefficient, which depends on the plate's support conditions and the applied stress.

$$4. \quad b_{\text{eff}} = \rho b$$

$$5. \quad \rho = 1.00 \quad \text{for} \quad \bar{\lambda}_p \leq 0.673$$

$$6. \quad \rho = \frac{(\bar{\lambda}_p - 0.22)}{\bar{\lambda}_p^2} \quad \text{for} \quad \bar{\lambda}_p > 0.673$$

$$7. \quad \bar{\lambda}_p = \frac{b}{28.4 \sqrt{k_c t \epsilon}}$$

Having determined the effective width of each element of the cross-section, the effective cross-sectional area (A_{eff}) is evaluated, which, multiplied by the yield stress, gives the cross-section compressive resistance. The buckling coefficient k_c employed in the plate slenderness formula of Equation 7 is taken as equal to four for internal elements in compression, assuming simply supported edges for the plates of both SHSs and RHSs. However, with increasing cross-section aspect ratio, the slender webs of a RHS are more effectively restrained against local buckling by the shorter (hence stockier) flanges. This is neglected in current European design provisions and each plate element is treated in isolation.

For RHSs with fully effective flanges (i.e. shorter faces), the actual reduction factor of the web (ρ_w) as obtained from the FE results is derived from Equation 8

$$8. \quad \rho_w = \frac{N_{u,FE} - f_y A_c - 2f_y b_f t}{2f_y b_w t}$$

where $N_{u,FE}$ is the numerical failure load of the modelled stub column, A_c is the area of the corner region, which is assumed fully effective, b_f is the width of the fully effective flanges and b_w is the width of the slender webs (i.e. longer faces). When both the flanges and the webs are slender, the actual reduction factor of the most slender element (ρ_w) can be derived on the basis of the FE failure load assuming that the ratio of the flange to the web reduction factor (ρ_f/ρ_w) is equal to that specified in EN 1993-1-5 (CEN, 2006), according to Equation 9.

$$9. \quad \rho_w = \frac{N_{u,FE} - f_y A_c}{2f_y t [b_w + b_f (\rho_f/\rho_w)]}$$

In Figure 6(b) the reduction factor of the most slender constituent plate element (ρ_w) is plotted against the corresponding slenderness ($\bar{\lambda}_w$). As can be seen, even though safe predictions were achieved overall, more conservative predictions were obtained for sections with higher cross-section aspect ratios and less conservative predictions for the SHSs. The same conclusion can be drawn from Table 3, where increasing aspect ratio is shown to lead consistently to more conservative strength predictions. This is clearly due to the element interaction between plated elements of dissimilar slenderness. It is worth noting that, particularly for HSS, for which slender sections are becoming increasingly common due to the increased material strength, it is important for the design to ensure safe but not overly conservative predictions that could reduce the benefits of adopting HSS. A design approach offering consistently accurate predictions throughout a range of aspect ratios likely to occur in practice is thus warranted.

Table 3. Assessment of design methods for slender sections

Cross-section aspect ratio, H/B	Effective width equations	Effective cross-section method
	Equations 8 and 9	Proposed Equations 10–12
	$\rho_{w,EC3}/\rho_{w,FE}$	$\rho_{cs,Pred}/\rho_{cs,FE}$
1.00	0.97	0.97
1.25	0.95	0.96
1.50	0.94	0.95
2.00	0.90	0.93
2.50	0.88	0.95
3.00	0.85	0.95
Mean	0.91	0.95
CoV	0.07	0.04

3.2 Effective cross-section method for slender sections

Based on the effective width equations applied to constituent plate elements of sections prone to local buckling, a method providing a reduction factor for the gross cross-sectional area has been proposed for slender stainless steel sections (Bock and Real, 2015; Zhou *et al.*, 2013b). This method, called the effective cross-section method herein, expresses the reduction factor as a function of the plate slenderness ($\bar{\lambda}_p$) and the cross-section aspect ratio (H/B), thus allowing for the influence of element interaction on the cross-sectional response. The method applies to both S460 and S690 slender stub columns.

Aiming to relate the cross-section reduction factor (ρ_{cs}) to both the plate slenderness and the cross-section aspect ratio, an equation relating the numerical compressive capacities normalised by the yield load (excluding the contribution of the corner regions, which are assumed not to undergo local buckling) to the slenderness ($c/t\epsilon$) of the most slender element for all class 4 sections was derived for each aspect ratio. The cross-section reduction factor has the general form of the Winter curve (Winter, 1947) and is given by

$$\rho_{cs} = \frac{\bar{\lambda}_p - C}{\bar{\lambda}_p^D} = \frac{[c/(28.4(k_c)^{1/2}t\epsilon)] - C}{[c/(28.4(k_c)^{1/2}t\epsilon)]^D} \quad (10)$$

$$= \frac{[c/(56.8t\epsilon)] - C}{[c/(56.8t\epsilon)]^D}$$

where C and D are coefficients depending on the cross-section aspect ratio H/B and k_c is the buckling coefficient as defined in EN 1993-1-5 (CEN, 2006). A linear regression analysis was conducted for each of the cross-section aspect ratios considered and the C and D values were obtained. Subsequently, empirical Equations 11 and 12, relating C and D to the aspect ratio H/B , were determined, as shown in Figure 7(a).

$$11. \quad C = 0.083(H/B)^{-2.325} + 0.123$$

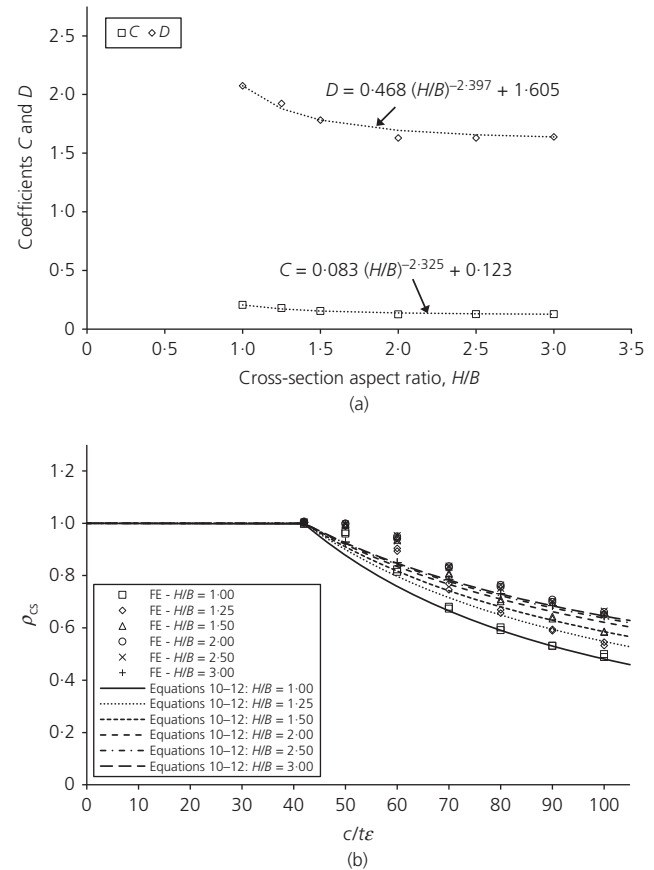


Figure 7. Proposed effective cross-section method for class 4 sections: (a) determination of coefficients C and D ; (b) reduction factor ρ_{cs} against $c/t\epsilon$

$$12. \quad D = 0.468(H/B)^{-2.397} + 1.605$$

Incorporating Equations 11 and 12 in Equation 10, the effective cross-section curves can be derived as a function of both the cross-section aspect ratio and the slenderness $c/t\epsilon$. As shown in Figure 7(b) and Table 3, the proposed Equations 10–12 yield accurate strength predictions, since they explicitly allow for the interaction between the constituent plate elements of hot-finished hollow sections. To further evaluate the accuracy of the effective cross-section method, test data on HSS concentric stub columns collated from the literature were used (Im *et al.*, 2005; Rasmussen and Hancock, 1992; Sakino *et al.*, 2004; Yoo *et al.*, 2013). The results are summarised in Table 4, revealing the capability of the proposed method to predict accurate design estimations for both SHS and RHS slender cross-sections.

3.3 Continuous strength method for stocky sections

In order to obtain accurate strength predictions over the full slenderness range, a rational exploitation of the strain-hardening exhibited for sections in S460 material in the stocky

Table 4. Assessment of the effective cross-section method for collated data (concentric stub columns, class 4 box cross-sections)

	Aspect ratio, H/B	Number of tests	Measured f_y : N/mm ²	$\rho_{cs, Pred}/\rho_{cs, Exp}$	
				Mean	CoV
Rasmussen and Hancock (1992)	1.00 (SHS)	2	670	0.94	0.04
Sakino <i>et al.</i> (2004)	1.55–2.36 (RHS)	4	540–835	0.98	0.01
Im <i>et al.</i> (2005)	1.00 (SHS)	4	533	0.94	0.07
Yoo <i>et al.</i> (2013)	1.00 (SHS)	1	761	0.98	N/A

N/A, non-applicable

slenderness region was deemed necessary. To this end, the CSM, which was originally developed for stainless steel sections (Gardner, 2002) and later expanded to cover carbon steel and aluminium alloys (Foster *et al.*, 2015; Gardner and Ashraf, 2006; Su *et al.*, 2014), was extended to cover hot-finished cross-sections in S460 grade. The CSM is based on an empirical relationship between the cross-section slenderness and the strain at failure due to local buckling, which defines a so-called base curve, and assumes an elastic-linear hardening material response, thus allowing stresses in excess of the yield stress to be taken into account when designing very stocky cross-sections. It is only applicable to sections with cross-section slenderness $\bar{\lambda}_{cs} = (f_y/f_{cr})^{1/2} \leq 0.68$, which fail at an average stress beyond their yield stress (f_{cr} is the elastic critical buckling stress of the section). In this study, the elastic critical buckling stress of the cross-section was obtained from the expressions developed by Seif and Schafer (2010) after execution of finite-strip analysis on a large number of sections. The expressions take into account the effect of the element interaction on the elastic critical buckling stress. For hollow sections under pure compression, the equations are given by

$$13. \quad f_{cr} = k_b \frac{\pi^2 E}{12(1 - \nu^2)} \left(\frac{t}{b_c} \right)^2$$

$$14. \quad k_b = 4/(h_c/b_c)^{1.7}$$

where E is Young's modulus, ν is Poisson's ratio, h_c and b_c are the centreline depth and width of the section, respectively, t is the thickness of the plate material and k_b is the local buckling coefficient accounting for both boundary and loading conditions and including plate element interaction effects. Alternatively, the critical stress of the cross-section can be conservatively taken as the critical stress of its most slender plate element. Incorporating a continuous relationship between the cross-section slenderness and the cross-section deformation capacity, the cross-section compression resistance $N_{u, csm}$ can be evaluated from

$$15. \quad N_{u, csm} = A f_{csm} = A [f_y + E_{sh}(\epsilon_{csm} - \epsilon_y)]$$

$$16. \quad \frac{\epsilon_{csm}}{\epsilon_y} = \frac{0.25}{\bar{\lambda}_{cs}^{3.6}} \quad \text{but} \quad \frac{\epsilon_{csm}}{\epsilon_y} \leq 15$$

in which A is the cross-sectional area, ϵ_y is the strain at yield load, f_{csm} is the CSM failure stress, ϵ_{csm} is the strain at the CSM failure load and E_{sh} is the strain-hardening modulus. Thus, the method does not limit the maximum attainable stress of a cross-section to the yield stress, but allows for the strain-hardening exhibited by stocky sections that fail at high inelastic strains. The limit of 15 imposed on the $\epsilon_{csm}/\epsilon_y$ ratio relates to the ductility requirements and is in accordance with the minimum guaranteed ϵ_u value given in the relevant Eurocodes, EN 1993-1-1 (CEN, 2005) and EN 1993-1-4 (CEN, 2015) for carbon steel and stainless steel, respectively. The respective value for HSS is ten, since HSSs are usually associated with a lower ductility (EN 1993-1-12 (CEN, 2007)). This limit ensures that no tensile fracture occurs when applying the CSM to flexural members. Since the focus of this paper is the response of compressive members, where no tension fracture can occur, this limit is not applied here.

In order to assess the applicability of the CSM to S460 hollow sections, the ratio ϵ_u/ϵ_y , where ϵ_u is the strain at failure (defined as the end-shortening at failure load normalised by the initial stub column length) is plotted against the cross-section slenderness ($\bar{\lambda}_{cs}$) in Figure 8(a). The base curve given by Equation 16 is also depicted in the same figure. The current base curve does not provide a close approximation to the obtained numerical results, presumably due to differences between the response of materials with a Ramberg–Osgood type of behaviour (for which the base curve was originally developed) and materials with a yield plateau. Since the base curve does not follow the obtained results closely, a least-squares regression analysis was applied to the stub column results and a new base curve (Equation 17) was derived. However, further research is needed to support the use of this equation to other steel grades.

$$17. \quad \frac{\epsilon_{csm}}{\epsilon_y} = \frac{0.027}{\bar{\lambda}_{cs}^{2.63+9.94\bar{\lambda}_{cs}}}$$

Having developed the base curve, a material model capable of accounting for strain-hardening is required for implementation of the CSM. To this end, the assumption of a modest strain-hardening modulus $E_{sh} = 1/100$, as recommended by annex C of EN 1993-1-5 (CEN, 2006), was adopted. As shown in Figure 8(b), a very good approximation of the material

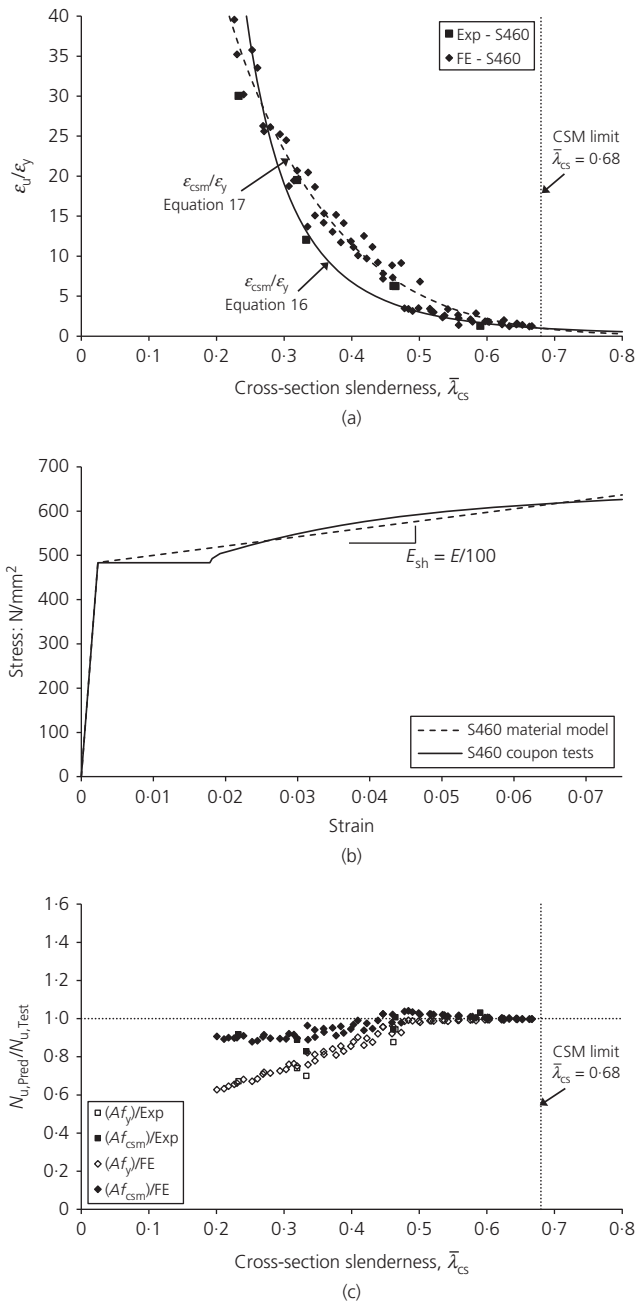


Figure 8. Assessment of the CSM for S460 sections with $\bar{\lambda}_{CS} \leq 0.68$: (a) ϵ_u/ϵ_y against cross-section slenderness $\bar{\lambda}_{CS}$; (b) assumed material model for the application of the CSM; (c) $N_{u,Pred}/N_{u,Test}$ against cross-section slenderness $\bar{\lambda}_{CS}$

response of S460 was achieved with the simplified bilinear model. More complicated material responses, including a trilinear approximation that accounted for the observed plateau, led to more involved design equations without a significant improvement in the accuracy of the strength predictions. The ultimate capacities obtained from the tests (Wang *et al.*, 2017) and the FE studies were then normalised by those predicted by the CSM and plotted against $\bar{\lambda}_{CS}$. The results are presented

Table 5. Assessment of the CSM for S460 sections with $\bar{\lambda}_{CS} \leq 0.68$

	FE results		Experimental results	
	$N_{u,EC3}/N_{u,FE}$	$N_{u,csm}/N_{u,FE}$	$N_{u,EC3}/N_{u,Exp}$	$N_{u,csm}/N_{u,Exp}$
Mean	0.82	0.97	0.88	0.94
CoV	0.17	0.05	0.14	0.08

in Figure 8(c), which shows a noticeable improvement in the accuracy of the CSM strength predictions compared with the Eurocode approach. This is also shown in Table 5, where more accurate design predictions – both in terms of achieved mean values and consistency – were attained with application of the CSM.

4. Reliability analysis

In order to assess the reliability of the proposed design methods, a statistical analysis following the provisions of annex D EN 1990 (CEN, 2002) was conducted. In particular, the CSM method and the effective cross-section method were statistically validated. Table 6 summarises the following key statistical parameters: the number of tests and FE simulations (n), the design (ultimate limit state) fractile factor ($k_{d,n}$), the average ratio of test (or FE) to model resistance based on a least-squares fit to all the data (\bar{b}), the CoV of the tests and FE simulations relative to the resistance model (V_δ), the combined CoV incorporating both model and basic variable uncertainties (V_T) and the partial safety factor for cross-section resistance (γ_{M0}). Based on the reliability analysis considerations provided in Wang *et al.* (2016), the material over-strength of HSS was taken equal to 1.135 with a CoV of 0.055, while the CoV of geometric properties was assumed to be equal to 0.02. The variation between the experimental and the numerical results (0.052) was also considered. Performing a first-order reliability method in accordance with the Eurocode target reliability requirements, the partial factors γ_{M0} were evaluated. As shown in Table 6, γ_{M0} was found to be lower than unity, indicating that the currently adopted value (i.e. $\gamma_{M0} = 1.00$) could be safely applied for the proposed design methods.

5. Conclusions

The compressive responses of S460 and S690 SHSs and RHSs were studied over a wide range of cross-section slenderness values. Test results from 11 concentric stub columns were used to validate the developed FE models. The experimental initial stiffness, ultimate loads and failure modes were successfully replicated by the FE models, which were then used to conduct parametric studies. Six aspect ratios and various thicknesses were adopted for both steel grades, thus leading to $c/t\epsilon$ varying between 10 and 100. The results were used to assess the EC3 class 3 slenderness limit, which was found to be applicable to the studied HSS sections, and for an assessment of the design procedures for stocky and slender sections. Regarding the

Table 6. Summary of the reliability analysis for the proposed design methods

Design method	Reliability analysis parameters					
	n	$k_{d,n}$	\bar{b}	V_{δ}	V_r	γ_{Mo}
Effective cross-section method – Proposed Equations 10–12	95	3.196	1.050	0.043	0.089	0.960
CSM – Proposed Equation 17	73	3.229	1.055	0.056	0.099	0.992

design of slender sections, application of the EC3 effective width equations led to largely scattered values. Since EC3 determines the slenderness of the cross-section on the basis of its most slender element, the effect of the interaction of the constituent plate elements was not taken into account. Element interaction was shown to be pronounced in hollow sections with high cross-section aspect ratios in the slender region. The application of an effective cross-section concept, where a reduction factor is applied on the whole cross-section and is based on the cross-section slenderness rather than on isolated plate elements, was developed and shown to give good results for both the HSS sections studied in this work and test data collated from the literature. For stocky sections in S460, the Eurocode predictions were deemed overly conservative, while for cross-sections in S690, which exhibited limited strain-hardening, the Eurocode predictions were appropriate. The applicability of the CSM was therefore extended to S460 hollow sections and was found to lead to safe yet more economic and consistent strength predictions and hence more efficient design. Both proposed design methods were statistically validated according to annex D of EN 1990 (CEN, 2002). Further research is needed to generalise the applicability of the design approaches to other HSS grades and facilitate their incorporation in future revisions of EN 1993-1-12 (CEN, 2007).

Acknowledgement

The research leading to these results received funding from the Research Fund for Coal and Steel (RFCS) under grant agreement RFSR CT 2012-00028.

REFERENCES

- AISC (American Institute of Steel Construction) (2010) ANSI/AISC 360-10: Specification for structural steel buildings. AISC, Chicago, IL, USA.
- AISI (American Iron and Steel Institute) (2012) AISI S100-12: North American specification for the design of cold-formed steel structural members. AISI, Washington, DC, USA.
- Bock M and Real E (2015) Effective width equations accounting for element interaction for cold-formed stainless steel square and rectangular hollow sections. *Structures* **2**: 81–90, <https://doi.org/10.1016/j.istruc.2015.02.003>.
- CEN (European Committee for Standardization) (2002) EN 1990: Eurocode–basis of structural design. CEN, Brussels, Belgium.
- CEN (2005) EN 1993-1-1: Eurocode 3: design of steel structures. Part 1-1: general rules and rules for buildings. CEN, Brussels, Belgium.
- CEN (2006) EN 1993-1-5: Eurocode 3: design of steel structures. Part 1-5: plated structural elements. CEN, Brussels, Belgium.
- CEN (2007) EN 1993-1-12: Eurocode 3: design of steel structures. Part 1-12: additional rules for the extension of EN 1993 up to steel grades S700. CEN, Brussels, Belgium.
- CEN (2015) EN 1993-1-4: 2006+A1: Eurocode 3: design of steel structures. Part 1-4: general rules – supplementary rules for stainless steels, including amendment A1. CEN, Brussels, Belgium.
- Dawson RG and Walker AC (1972) Post-buckling of geometrically imperfect plates. *Journal of the Structural Division ASCE* **98**(1): 75–94.
- Foster ASJ, Gardner L and Wang Y (2015) Practical strain-hardening material properties for use in deformation-based structural steel design. *Thin-Walled Structures* **92**: 115–129, <https://doi.org/10.1016/j.tws.2015.02.002>.
- Galambos TV (1998) *Guide to Stability Design Criteria for Metal Structures*, 5th edn. Wiley, New York, NY, USA.
- Gao L, Sun H, Jin F and Fan H (2009) Load-carrying capacity of high-strength steel box-sections I: stub columns. *Journal of Constructional Steel Research* **65**(4): 918–924.
- Gardner L (2002) *A New Approach to Stainless Steel Structural Design*. PhD thesis, Imperial College London, London, UK.
- Gardner L and Ashraf M (2006) Structural design for non-linear metallic materials. *Engineering Structures* **28**(6): 926–934.
- Gardner L and Nethercot DA (2004) Numerical modeling of stainless steel structural components – a consistent approach. *Journal of Structural Engineering* **130**(10): 1586–1601.
- Gardner L, Saari N and Wang FC (2010) Comparative experimental study of hot-rolled and cold-formed rectangular hollow sections. *Thin-Walled Structures* **48**(7): 495–507.
- Gkantou M, Wang J, Theofanous M, Gardner L and Baniotopoulos C (2017) Structural behaviour of high strength steel hollow sections under compression and uniaxial bending. *Proceedings of the Institution of Civil Engineers*, in press.
- Hibbit, Karlsson & Sorensen Inc. (2010) *Abaqus/Standard User's Manual Volume III and Abaqus CAE Manual. Version 6.10*. Hibbit, Karlsson & Sorensen Inc., Pawtucket, RI, USA.
- Im SW, Kim YS and Chang IH (2005) A study on the characteristics of SM570TMC plates in compression members. *Journal of the Korean Society of Steel Construction* **17**(3): 357–363.
- Kim DK, Lee CH, Han KH et al. (2014) Strength and residual stress evaluation of stub columns fabricated from 800MPa high-strength steel. *Journal of Constructional Steel Research* **102**: 111–120, <https://doi.org/10.1016/j.jcsr.2014.07.007>.
- Nishino F, Ueda Y and Tall L (1966) *Experimental Investigation of the Buckling Plates with Residual Stress*. Lehigh University, Bethlehem, PA, USA, Fritz Engineering Laboratory Report 290.3.
- Rasmussen KJR and Hancock GJ (1992) Plate slenderness limits for high strength steel sections. *Journal of Constructional Steel Research* **23**(1): 73–96.
- Sakino K, Nakahara H, Morino S and Nishiyama I (2004) Behavior of centrally loaded concrete-filled steel-tube short columns. *Journal of Structural Engineering* **130**(2): 180–188.
- Seif M and Schafer BW (2010) Local buckling of structural steel shapes. *Journal of Constructional Steel Research* **66**(10): 1232–1247.

- Shi G, Zhou W, Bai Y and Lin C (2014) Local buckling of 460MPa high strength steel welded section stub columns under axial compression. *Journal of Constructional Steel Research* **100**: 60–70, <https://doi.org/10.1016/j.jcsr.2014.04.027>.
- Shi G, Xu K, Ban H and Lin C (2016) Local buckling behavior of welded stub columns with normal and high strength steels. *Journal of Constructional Steel Research* **119**: 144–153, <https://doi.org/10.1016/j.jcsr.2015.12.020>.
- Standards Australia (2012) AS 4100-A1: Amendment no.1 to AS 4100–1998 steel structures. Standards Australia, Sydney, Australia.
- Su MN, Young B and Gardner L (2014) Deformation-based design of aluminium alloy beams. *Engineering Structures* **80**: 339–349, <https://doi.org/10.1016/j.engstruct.2014.08.034>.
- Usami T and Fukumoto Y (1984) Welded box compression members. *Journal of Structural Engineering* **110(10)**: 2457–2470.
- Wang J, Afshan S, Gkantou M et al. (2016) Flexural behaviour of hot-finished high strength steel square and rectangular hollow sections. *Journal of Constructional Steel Research* **121**: 97–109, <https://doi.org/10.1016/j.jcsr.2016.01.017>.
- Wang J, Afshan S, Schillo N et al. (2017) Material properties and compressive local buckling response of high strength steel square and rectangular hollow sections. *Engineering Structures* **130**: 297–315, <https://doi.org/10.1016/j.engstruct.2016.10.023>.
- Winter G (1947) Strength of thin steel compression flanges. *Transactions of the American Society of Civil Engineers* **112(1)**: 527.
- Yang D and Hancock GJ (2004) Compression tests of cold-reduced high strength steel sections. I: stub columns. *Journal of Structural Engineering* **130(11)**: 1772–1781.
- Yoo JH, Kim JW, Yang JG, Kang JW and Lee MJ (2013) Local buckling in the stub columns fabricated with HSA800 of high performance steel. *International Journal of Steel Structures* **13(3)**: 445–458.
- Yuan B (1997) *Local Buckling of High Strength Steel W-Shaped Sections*. McMaster University, Canada, Technical report, Paper 4059.
- Zhou F, Tong L and Chen Y (2013a) Experimental and numerical investigations of high strength steel welded H-section columns. *International Journal of Steel Structures* **13(2)**: 209–218.
- Zhou F, Chen Y and Young B (2013b) Cold-formed high strength stainless steel cross-sections in compression considering interaction effects of constituent plate elements. *Journal of Constructional Steel Research* **80**: 32–41, <https://doi.org/10.1016/j.jcsr.2012.09.004>.

How can you contribute?

To discuss this paper, please email up to 500 words to the editor at journals@ice.org.uk. Your contribution will be forwarded to the author(s) for a reply and, if considered appropriate by the editorial board, it will be published as discussion in a future issue of the journal.

Proceedings journals rely entirely on contributions from the civil engineering profession (and allied disciplines). Information about how to submit your paper online is available at www.icevirtuallibrary.com/page/authors, where you will also find detailed author guidelines.